Supplementary Information for

Polarization-Sensitive Photothermoelectric Photodetector Based on Mixed-Dimensional SWCNT-MoS₂ Heterostructures

Pei-Yu Huang[a], Hong-Ji Chen[a], Jing-Kai Qin[a,*], Liang Zhen[a,b] and Cheng-Yan Xu[a,b,*]

[a] Sauvage Laboratory for Smart Materials, School of Materials Science and Engineering, Harbin Institute of Technology (Shenzhen), Shenzhen 518055, China

[b] MOE Key Laboratory of Micro-System and Micro-Structures Manufacturing, Harbin Institute of Technology, Harbin 150080, China

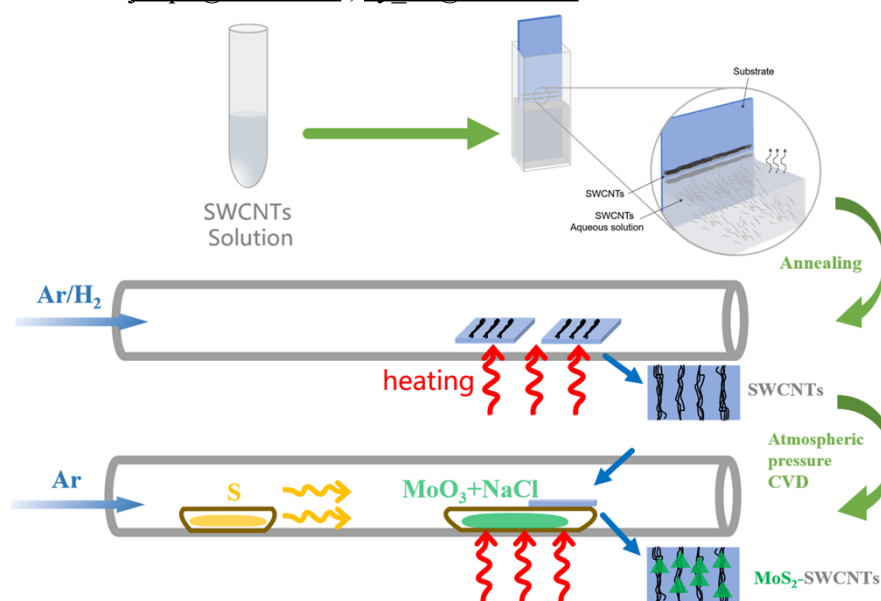[*] E-mail addresses: jk.qin@hit.edu.cn ; cy_xu@hit.edu.cn

Fig. S1 Schematic diagram for SWCNT-MoS₂ hybrid films preparation.
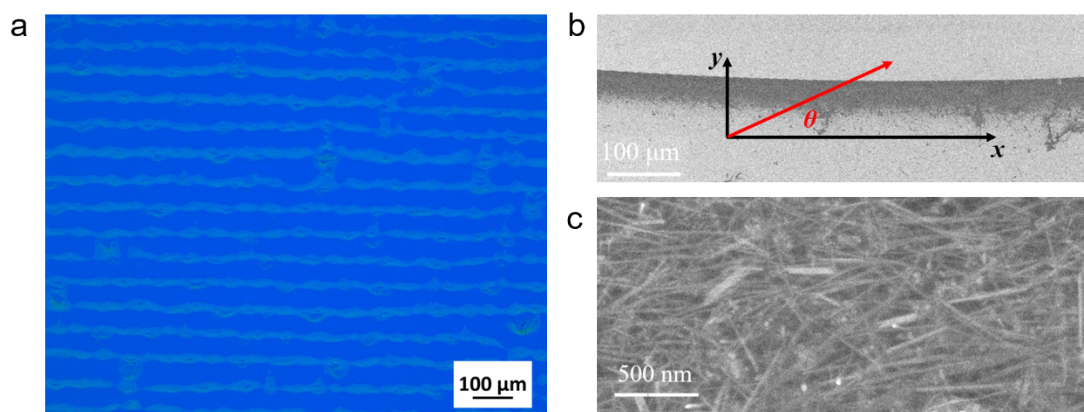

Fig. S2 Structural characterization of as-fabricated bare SWCNT films. (a) Optical image of the SWCNT films on SiO₂/Si substrate. (b) SEM and (c) magnified SEM image of the SWCNT films.
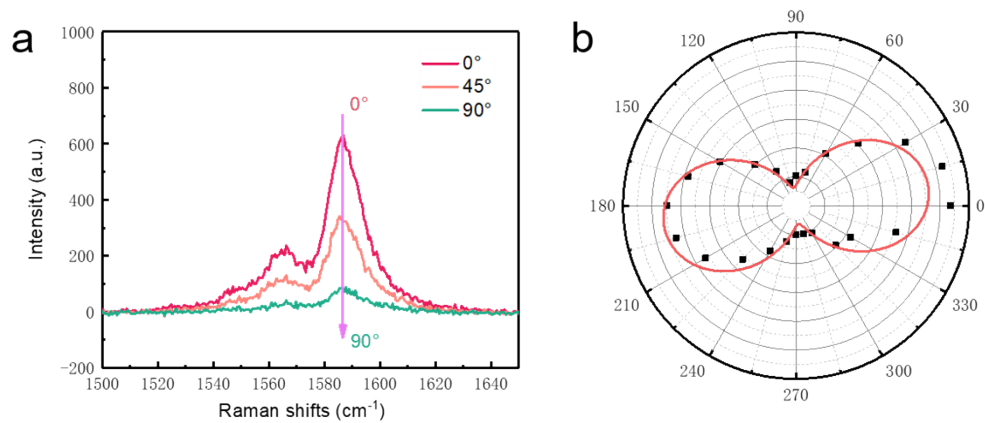
Fig. S3 Polarization-resolved Raman spectra for SWCNT films. (a) Polarization-sensitive Raman spectrum of aligned film. (b) Polar coordinates of the Polarization-resolved Raman spectra of G mode.
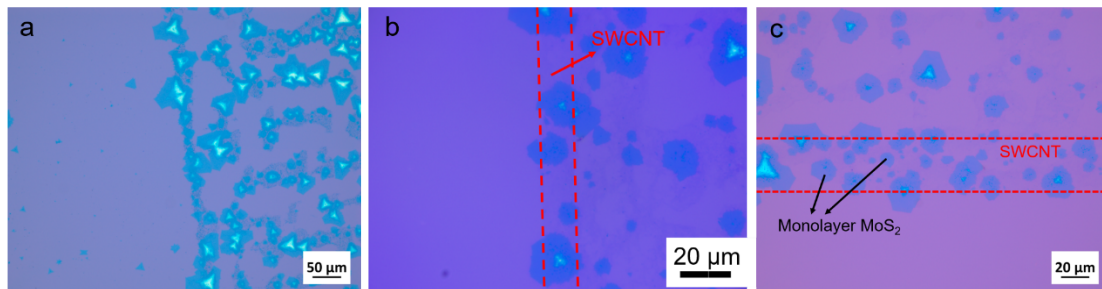

Fig. S4 Structural characterization of as-fabricated SWCNT-MoS_2 hybrid films. (a) Optical image of continuous MoS_2 film along the parallel direction of SWCNT strips on SiO_2/Si substrate. (b-c) Individual MoS_2 nanosheet distribute on SWCNT films.
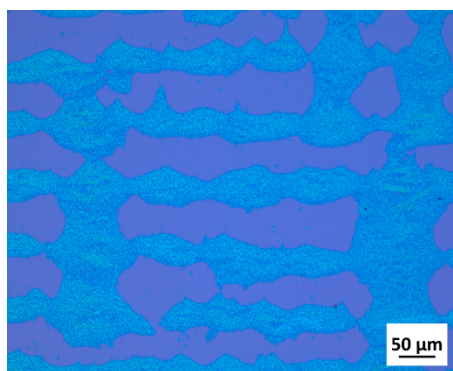

Fig. S5 The morphology of SWCNT-MoS_2 hybrid films without hydrogen annealing process.
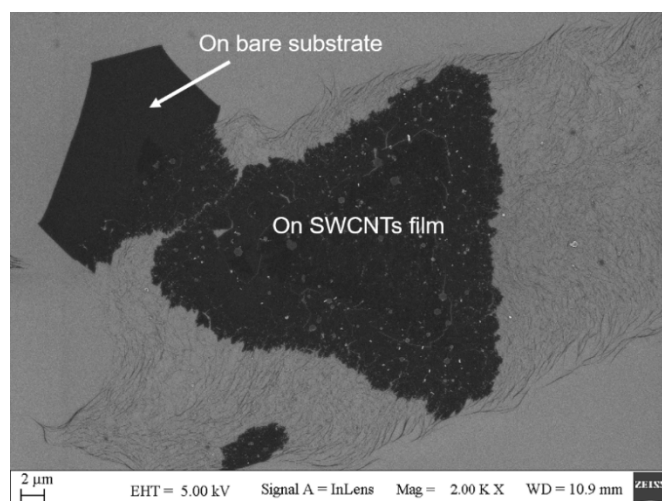
Fig. S6 The morphology of monolayer MoS_2 on different substrates.
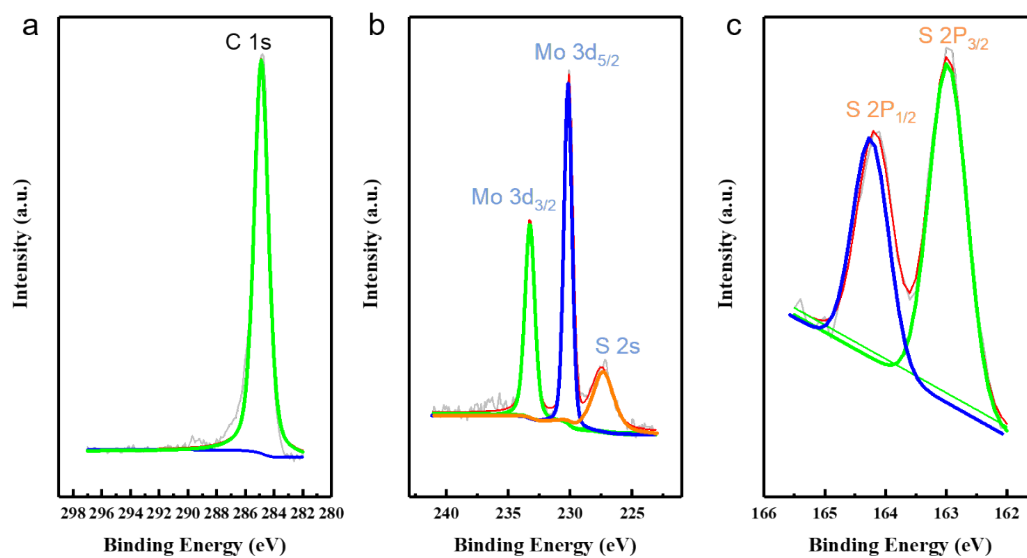

Fig. S7 Chemical composition of SWCNT-MoS_2 hybrid films. (a) C 1s, (b) Mo 3d and (c) S 2p XPS characteristic peak.
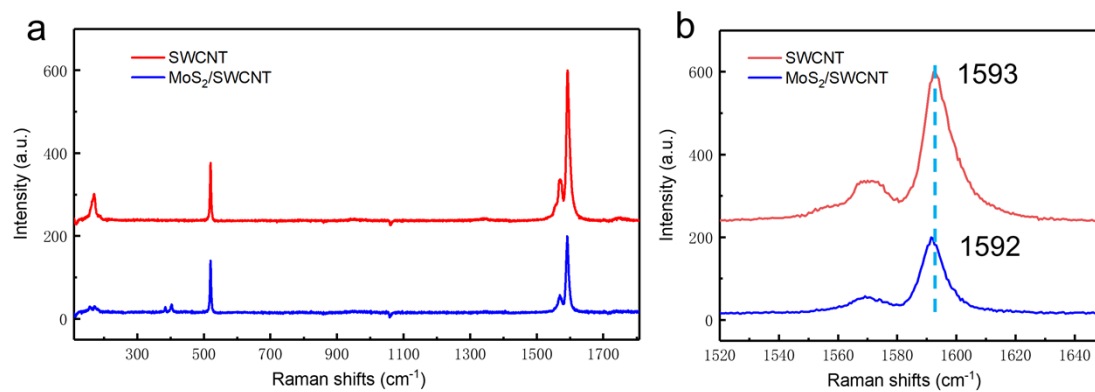

Fig. S8 Raman spectra of SWCNT-MoS_2 hybrid films. (a) Wide range and (b) magnified Raman spectra for SWCNT-MoS_2 hybrid structures.
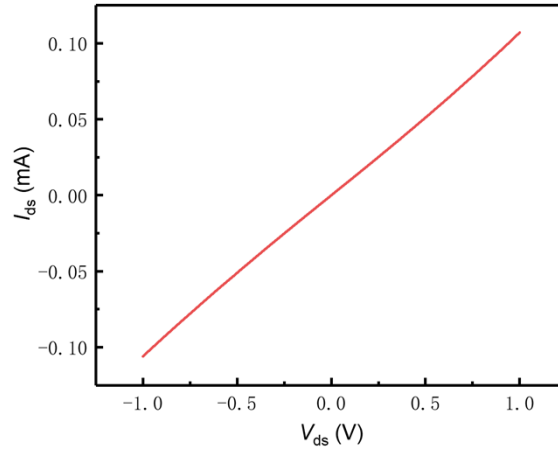
Fig. S9 I_{ds}-V_{ds} characteristic of the PTE detector with wide range from -1V to 1V at dark condition.
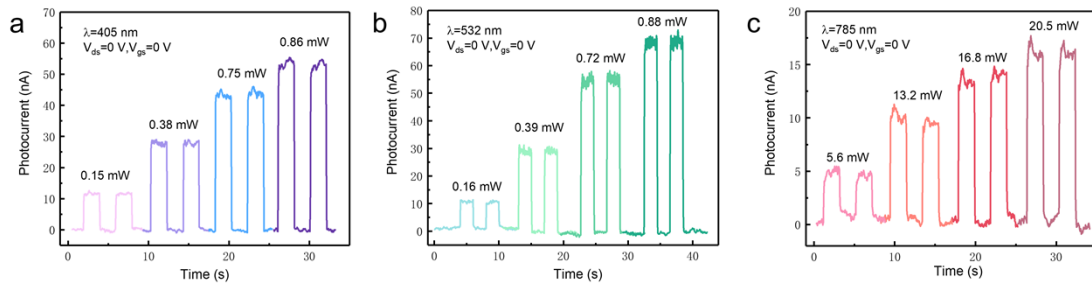

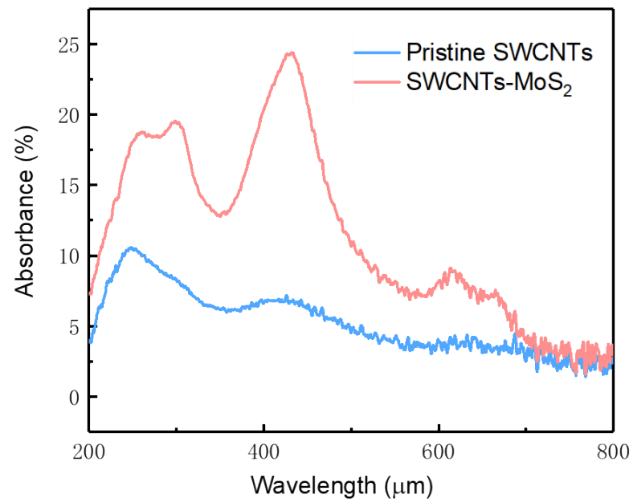**Fig. S10** Photoresponse of the device under different 405, 532, and 785 nm laser intensity, respectively.

Fig. S11 Absorption spectra of SWCNT-MoS$_2$ hybrid films and pure MoS$_2$, respectively.
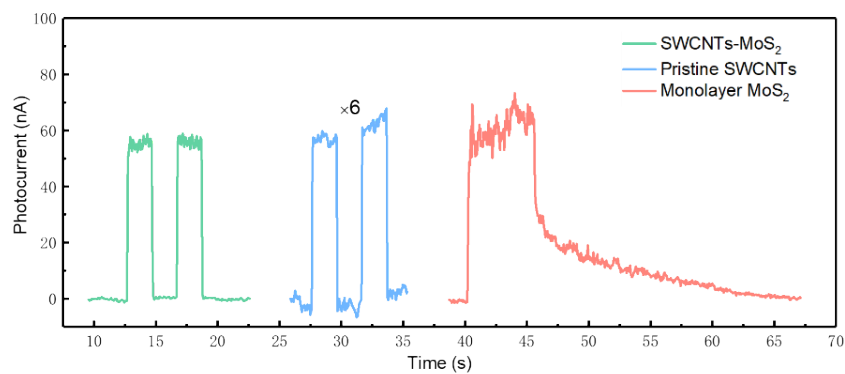
Fig. S12 Photoresponse of the SWCNT-MoS$_2$, monolayer MoS$_2$, and pristine SWCNT device at the same 532 nm laser intensity, respectively.
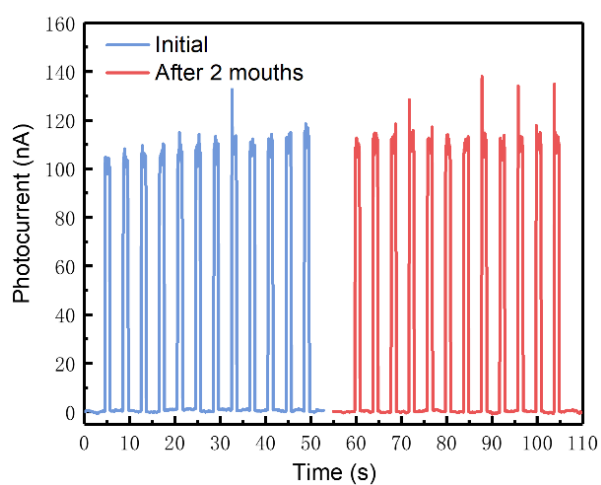

Fig. S13 The environmental stability of SWCNT-MoS$_2$ hybrid films after exposure to air for 2 months.

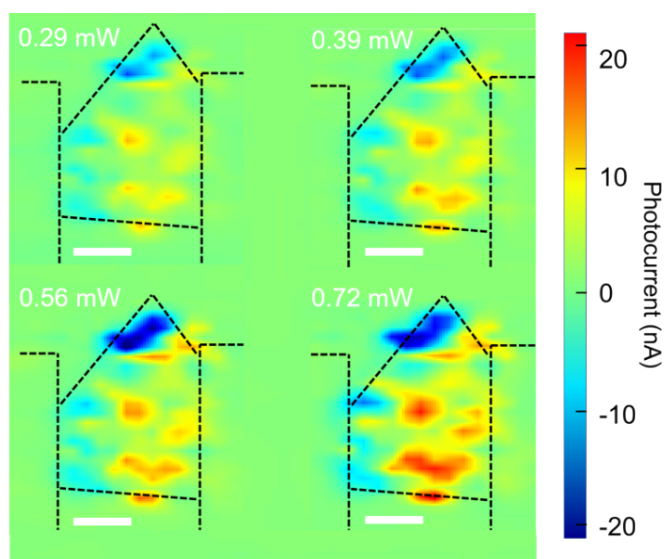**Fig. S14** Powder-dependent spatial distribution of photocurrent for hybrid structures. Scale bar: 2 μm.
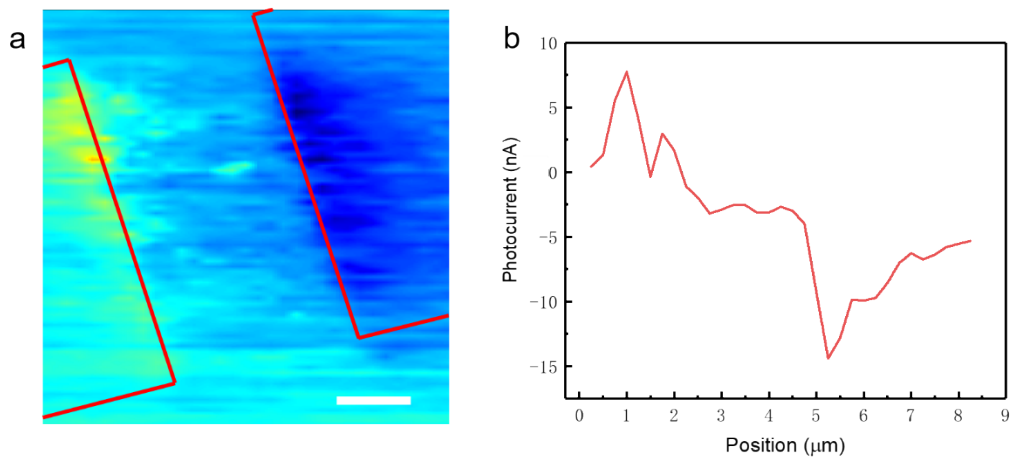
Fig. S15 Spatial distribution of photocurrent for bare SWCNT films. (a) SPCM of pristine SWCNT devices. (b) The current intensity profile of the same line cut along the center of channel. Scale bar: 2 μm.
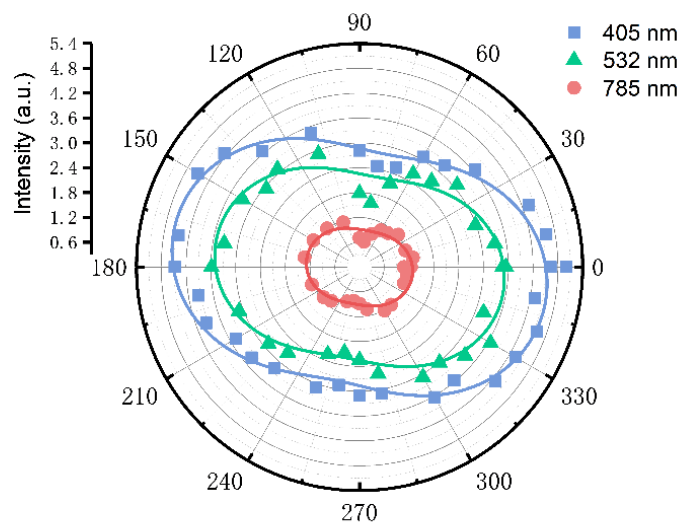

Fig. S16 Polar coordinates of the polarization-sensitive absorbance at 405, 532 and 785 nm.
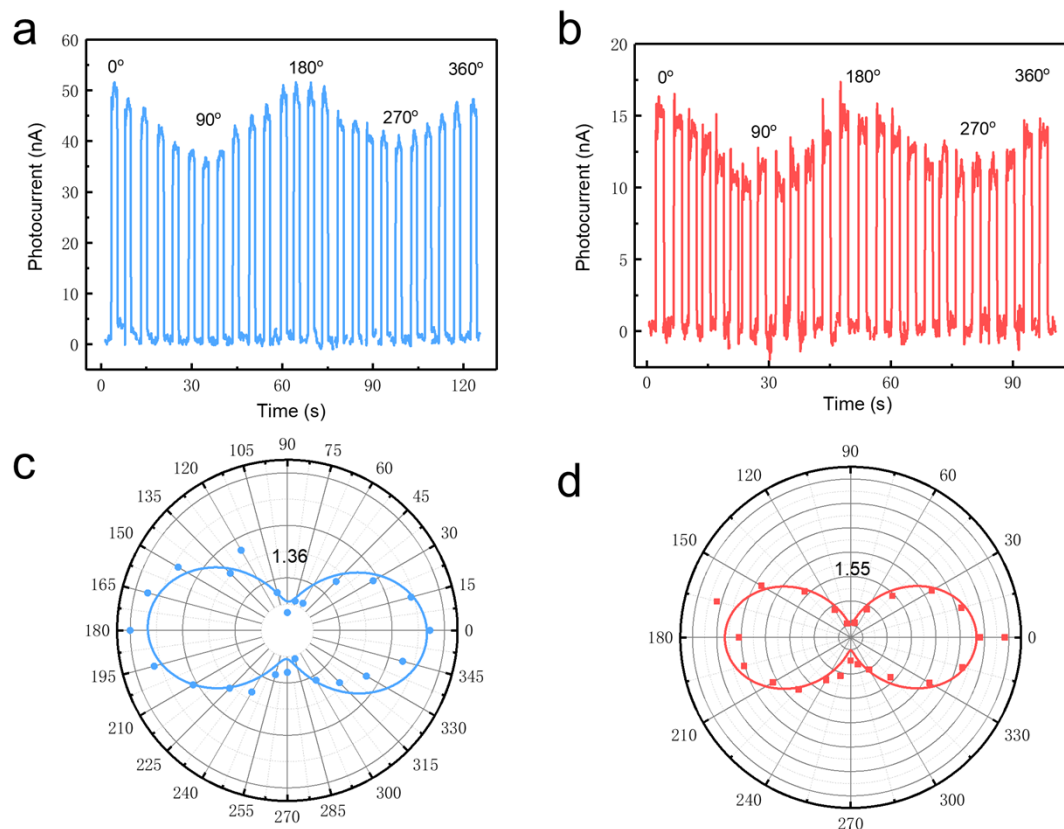
Fig. S17 Polarization-resolved photodetector based on SWCNT-MoS$_2$ hybrid films. (a-b) Light linear polarization dependence of photocurrent for 405 and 785 nm light illuminations, respectively. (c-d) Polar coordinates of the polarization-sensitive photoreponse at 405 and 785 nm illuminations, respectively.

Table S1 Comparison of state-of-art PTE photodetectors

Materials	Responsivity	Response speed	Spectral range	Polarization ratios	References
graphene	2.85 µA W^{-1}	4 ps		0	1
WTe$_2$	50 µA W^{-1}	0.22 ns	650-850 nm		2
TaIrTe$_4$	20 µA W^{-1}	27 µs	Vis-IR	1.13 (660 nm)	3
SWCNT film	28 mV W^{-1}	32 µs	Vis-IR	2 (660 nm)	4
p-n junction SWCNT film	1 V W^{-1}	0.6 s-90 µs	Vis-IR	1.28 (660 nm)	5
SWCNT-MoS$_2$	88 µA W^{-1}	~100 ms	405-785 nm	1.55 (532nm)	This work

Supplementary References

1 D. Sun, G. Aivazian, A. M Jones, J.S. Ross, W. Yao, D. Cobden and X.D. Xu, *Nat. Nanotechnol.*, 2012, **7**, 114-118.

2 Q. Wang, C. Yesilyurt, F. Liu, Z. B. Siu, K. Cai, D. Kumar, Z. Liu, M. B. A. Jalil and

H. Yang, *Nano Lett.*, 2019, **19**, 2647-2652.

3 J. Lai, Y. Liu, J. Ma, X. Zhuo, Y. Peng, W. Lu, Z. Liu, J. Chen and D. Sun, *ACS Nano*, 2018, **12**, 4055-4061.

4 S. Nanot, A. W. Cummings, C. L. Pint, A. Ikeuchi, T. Akiho, K. Sueoka, R. H. Hauge, F. Leonard and J. Kono, *Sci. Rep.*, 2013, **3**, 1335.

5 X. He, X. Wang, S. Nanot, K. Cong, Q. Jiang, A. A. Kane, J. E. Goldsmith, R. H. Hauge, F. Leonard and J. Kono, *ACS Nano*, 2013, **7**, 7271-7277.